PERGAMON

Journal of Structural Geology 25 (2003) 591–609

JOURNAL OF STRUCTURAL GEOLOGY

www.elsevier.com/locate/jstrugeo

Push-ups, fracture patterns, and palaeoseismology of the Leirubakki Fault, South Iceland

Françoise Bergerat[a,*], Jacques Angelier[a], Agust Gudmundsson[b], Helgi Torfason[c]

[a]*Laboratoire de Tectonique, UMR 7072 CNRS-UPMC, case 129, 4, place Jussieu, 75252 Paris cedex 05, France*
[b]*Geological Institute, University of Bergen, Allegaten 41, N-5007 Bergen, Norway*
[c]*National Energy Authority, Grensasvegur 9, IS-108 Reykjavik, Iceland*

Received 11 January 2001; received in revised form 31 January 2002; accepted 28 March 2002

Abstract

Field measurements and GPS mapping were conducted along the Leirubakki Fault, a 010°-trending right-lateral strike-slip fault located in the Holocene lava flows of the South Iceland Seismic Zone. Because of poor exposures south and north of the Holocene lava flow dissected by the fault, its length can only be traced for 7.5 km. The exposed surface rupture contains fractures that range in size over four orders of a magnitude, from the main fault, through fault segments (1000–2000 m long), fracture arrays (100–250 m long), to individual fractures (8–125 m long). Detailed measurements were made of 63 push-ups, located at junctions between individual fractures and between fracture arrays, and ranging in maximum height from 0.35 to 4.35 m. Using the push-ups, the maximum right-lateral displacement on the Leirubakki Fault is estimated at 2.67 m. Using empirical relationships established globally, it is concluded that for a maximum displacement of 2.67 m, the true rupture length of the Leirubakki Fault is around 50 km and that it gave rise to an earthquake of a moment magnitude 7.1.

Keywords: Push-ups; Fracture patterns; Palaeoseismology; Iceland

1. Introduction

Iceland is located on the Mid-Atlantic Ridge, between the Kolbeinsey Ridge in the north and the Reykjanes Ridge in the south (Fig. 1). The tectonic and magmatic activity in Iceland is controlled partly by its location above a major mantle thermal anomaly, the Iceland Mantle Plume, and partly by the spreading of the Mid-Atlantic Ridge. The plate separation in Iceland occurs along the N105°E direction with a rate of 1.8 cm/year, according to the NUVEL-1 global plate motion model (DeMets et al., 1990, 1994). The Iceland Mantle Plume is responsible for the large magmatic supply, and thus for the existence of Iceland and the relatively great thickness of its crust. Because the Mid-Atlantic Ridge is moving westwards with respect to the Iceland Plume, the rift system in Iceland has repeatedly been shifted eastwards during the Late Cenozoic. New rift zones developed in the region located above the Iceland Plume when the plate boundary had migrated to a critical distance from it.

These rift jumps have lead to the development of two major ocean-ridge discontinuities (here also referred to as transform zones), both of which are partly exposed on land. These discontinuities connect the rift zones of Iceland and the oceanic ridges, and are referred to as the Tjörnes Fracture Zone, in North Iceland, and the South Iceland Seismic Zone (Fig. 1). Both of these zones are presently characterised by high levels of seismotectonic activity. The Leirubakki earthquake rupture analysed here belongs to the South Iceland Seismic Zone.

The South Iceland Seismic Zone (SISZ), centred at 64°N, is located at the junction of three rift-zone segments, forming a complex pattern (Fig. 2). At the western tip of the SISZ, the Reykjanes Peninsula represents the on-land extension of the Reykjanes Ridge. The West Volcanic Zone represents the main rift-zone segment of Southwest Iceland. At the eastern tip of the SISZ is the East Volcanic Zone, the longest and most active rift segment of Iceland.

The activity of the East Volcanic Zone began 2–3 m.y. ago (Jóhannesson et al., 1990); earlier, the West Volcanic Zone was the single active rift zone in South Iceland.

* Corresponding author. Tel.: +33-1-44-27-34-43; fax: +33-1-44-27-50-85.
E-mail address: bergerat@lgs.jussieu.fr (F. Bergerat).

0191-8141/03/$ - see front matter © 2002 Elsevier Science Ltd. All rights reserved.
PII: S0191-8141(02)00051-2

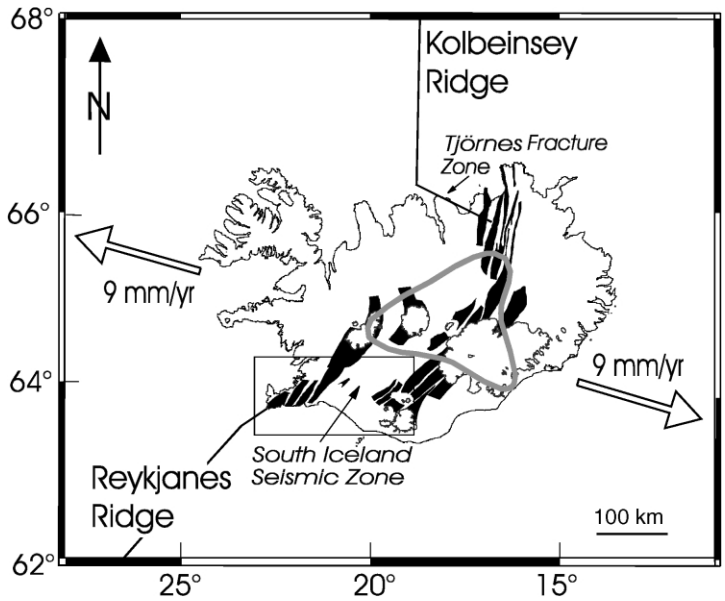

Fig. 1. Plate boundaries in Iceland and location of the South Iceland Seismic Zone. In black: main Holocene volcanic systems of the rift zones onshore (after Saemundsson, 1979). Thin lines offshore: ocean ridges north and south of Iceland. Open arrows indicate direction and velocity of plate divergence according to Nuvel-1 data from DeMets et al. (1990, 1994). In grey, postulated extension of the hot spot at 400 km depth (after Tryggvason et al., 1983). Thin rectangular frame in South Iceland: location of Fig. 2.

Ward (1971) proposed that the SISZ is an E–W left-lateral transform fault zone. There is, however, no major E–W-trending fault in South Iceland. Today, the SISZ is considered as a zone of high shear-stress concentration, located between the West Volcanic Zone and the East Volcanic Zone. Whether the SISZ will eventually develop into a transform fault or remain a zone between overlapping rift-zone segments is, as yet, unknown. For periods of years or decades, the (micro-)seismicity of the SISZ is essentially confined to a zone that is about 20 km wide (N–S) and 70 km long (E–W) (Fig. 2). However, when there are major destructive earthquakes in the SISZ, its N–S width is likely to be many tens of kilometres (Gudmundsson, 1995). During the last few centuries, several sequences of large earthquakes (M = 6–7) occurred in the SISZ at intervals of 45–112 years. These earthquakes have mostly been associated with N–S-trending right-lateral strike-slip faults arranged parallel and closely spaced (Einarsson et al., 1981; Einarsson and Eiriksson, 1982b).

We focus this study on the Leirubakki earthquake

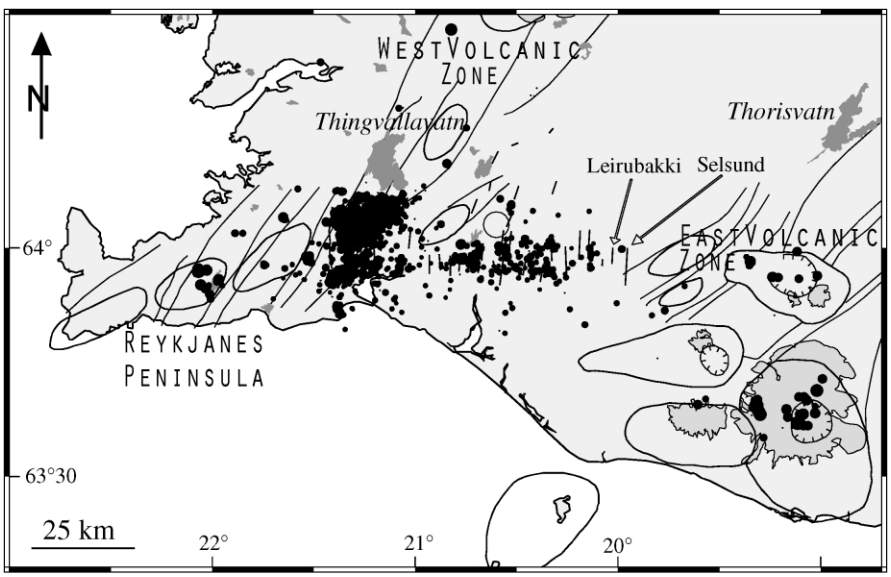

Fig. 2. General structure and seismicity of the South Iceland Seismic Zone and surrounding areas. Thin lines trending NE–SW: boundaries of fissure swarms in the rift segments. Roughly elliptical areas: outlines of the main Holocene volcanic systems (after Saemundsson, 1979). Black dots: selected earthquakes with magnitudes larger than 0.5 during the year 1995 (after Bergerat et al., 1998, from the SIL network; see Stefánsson et al., 1993). Dark grey area: lakes. Thin straight lines trending N–S: main seismogenic dextral strike-slip faults in the SISZ after Einarsson (1991).

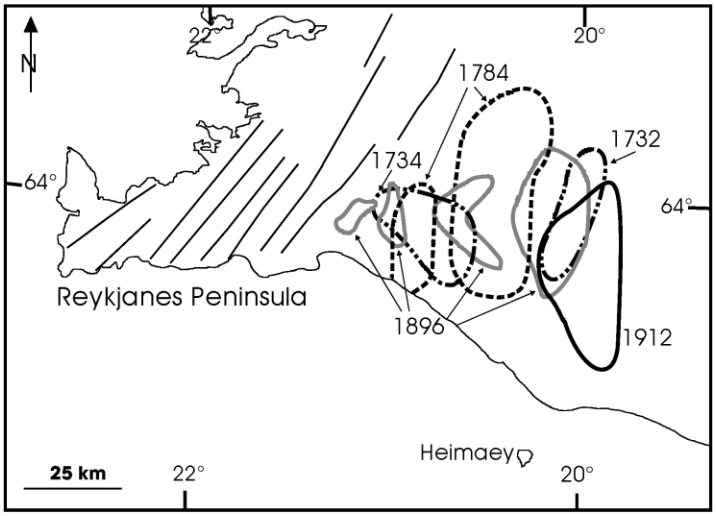

Fig. 3. Map of the South Iceland seismic Zone showing the destruction zones of the major earthquakes since 1700 (after Einarsson and Björnsson, 1979). In these zones more than 50% of houses at each farm were ruined. Thin lines trending NE–SW: main faults of fissure swarms in the rift segments.

rupture, a typical N–S-trending strike-slip fault located in the eastern part of the SISZ, a few kilometres west of the site of another large N–S-trending fault corresponding to the last major historical earthquake that occurred in 1912 in the SISZ: the M7 Selsund earthquake (Einarsson et al., 1981; Einarsson and Eiriksson, 1982a,b; Bjarnason et al., 1993) discussed in more detail in Section 6. The first aim of this paper is to present very detailed maps of the central part of the Leirubakki Fault and to describe accurately the characteristic system of fractures and push-ups. The second aim is to use these field measurements to quantify some important paleoseismological parameters of this earthquake rupture, such as its total length, the fault displacement, and the magnitude of the associated main shock. By placing the Leirubakki Fault within the structural framework of the SISZ, we aim at contributing to a better understanding of the present-day seismotectonic mechanical behaviour of this seismic zone.

2. Historical seismicity pattern of the South Iceland Seismic Zone

Written documents concerning the main catastrophic earthquakes exist since the settlement of Iceland in the 9th century. However, before 1700, the quality and reliability of these accounts are disputable and sometimes incomplete (Tryggvason et al., 1958). Reports are missing for the period 1400–1500, which corresponds to a difficult period in the history of Iceland, with two disastrous epidemics of plague. The first attempt at gathering all the available reports on earthquakes in a comprehensive study was made by Thoroddsen (1899, 1905, 1925). Later, Thorarinsson (in Tryggvason et al., 1958) and Einarsson et al. (1981) provided tables of destructive earthquakes (inducing the collapse of farmhouses). After 1700, the contemporary descriptions of earthquakes improved, making it possible to map the main destruction zones (Fig. 3). The seismic events of these last three centuries were described by several authors (e.g. Bjornsson, 1975, 1978; Einarsson and Björnsson, 1979; Stefánsson, 1979; Halldorsson et al., 1984). Except for the magnitude of the 1912 Selsund earthquake, which was instrumentally determined at $M = 7$ (Karnik, 1969), the magnitudes of the destructive earthquakes of these three last centuries are not known.

In addition to describing the destruction, fault ruptures are mentioned in association with the earthquakes of 1294, 1308, 1339, 1391, 1630, 1784, 1896 and 1912 (Thoroddsen, 1899, 1905; Einarsson et al., 1981; Einarsson and Eiriksson, 1982a,b). Other fault ruptures at the surface of the SISZ are generally of an unknown age. The Leirubakki Fault is one of these undated faults. Because of the large size of the observable features along the fault trace (larger than those of the M7 Selsund earthquake of 1912), it is likely that the Leirubakki earthquake was a major one. There is no information about it, so that the only possible period for this earthquake to have occurred in historical time is the 15th century, because of the lack of written accounts mentioned before. However, even in this poorly documented century, a major earthquake producing such a large rupture trace would probably have been recorded (R. Stefansson, pers. comm., 2000). On this view, the Leirubakki earthquake is probably older than the historical period, that is, older than 1100 years.

Both the initial rupture architecture and the subsequent preservation of the seismic fault traces within the SISZ depend much on the geological nature of the surface (soil, moraines, aa or pahoehoe lava flows, glacial–fluvial deposits). Despite this variety, certain characteristic features can be recognised along most of the faults (Einarsson et al., 1981). Several major faults, such as those associated with the earthquake ruptures of 1630, 1896 and 1912, have been

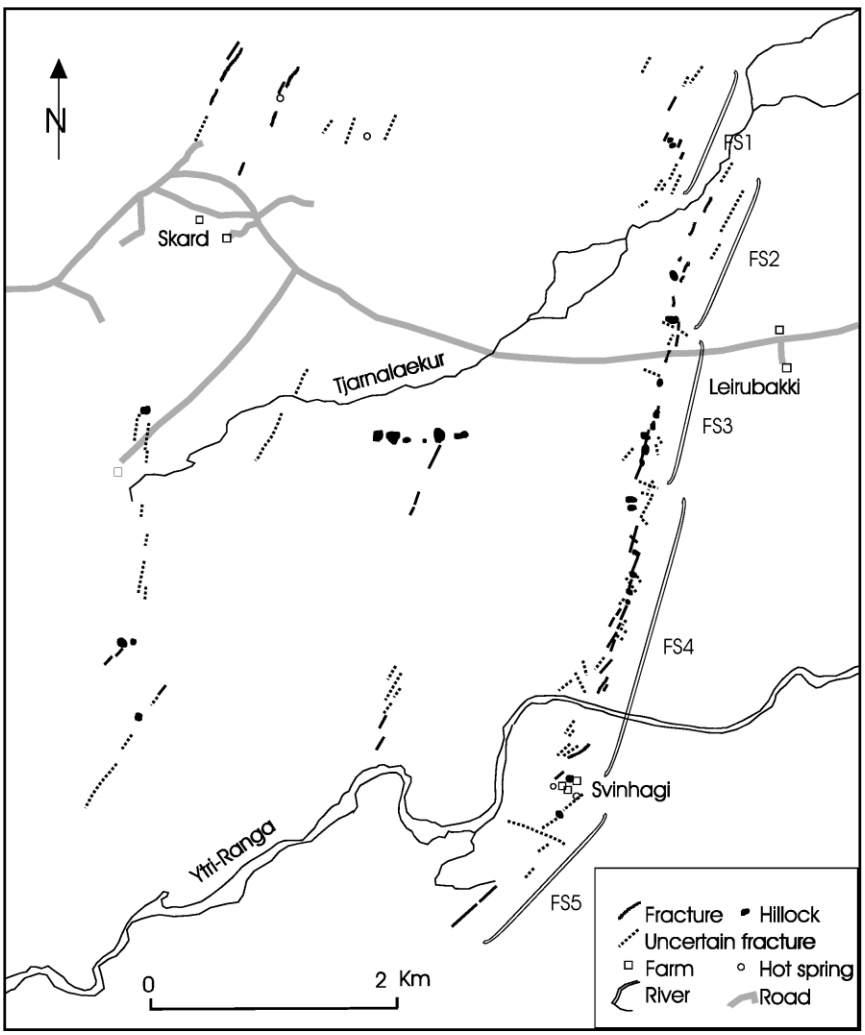

Fig. 4. Map of the Leirubakki Fault drawn from aerial photographs. FS1–FS5 represent five main fault segments of the Leirubakki Fault. Scattered traces of some other large seismic faults are also visible west of the Leirubakki fault.

mapped and described by Einarsson et al. (1981), Einarsson and Eiriksson (1982a,b) and Bjarnason et al. (1993). These descriptions are based on written records, interviews of inhabitants, studies of aerial photographs, and observations and measurements in the field.

3. Methodology

In order to quantify the geometry of the Leirubakki Fault at different scales, we adopted three different approaches. First, a general map of the fault trace was drawn based on aerial photographs (Fig. 4) and completed with pictures and observations during an aerial inspection of the area (Fig. 5). These data allowed us to identity the main features of the entire fault trace.

Second, detailed mapping of the central part of the fracture system associated with the Leirubakki Fault was made with a Trimble GPS Pathfinder Pro XRS differential system (Fig. 6). The GPS receiver automatically calculates with sub-metric accuracy, and stores the positions of different features of interest, such as particular points, lines, and areas. This allowed the positions, shapes and elevations of all fault-related structures to be accurately measured and recorded. We post-processed the carrier phase data in order to obtain an accuracy better than 10 cm (1–2 cm in the horizontal plane, and 2–5 cm in the vertical plane). Thus, the GPS technique allowed us to map in great detail the surface rupture of the Leirubakki Fault along its central, and most interesting, part (Fig. 6). The high resolution of the differential GPS implies that the measurement uncertainties are negligible with respect to the estimated measurement errors of the ordinary field observations. Because of the rugged lava flow surface masking the topographic expression of the tectonic features, or of recent soils or sands where most of the tectonic surface features have disappeared, the differential GPS mapping was not carried out in the northern and southern segments of the fault trace.

Third, we analysed some characteristic deformation

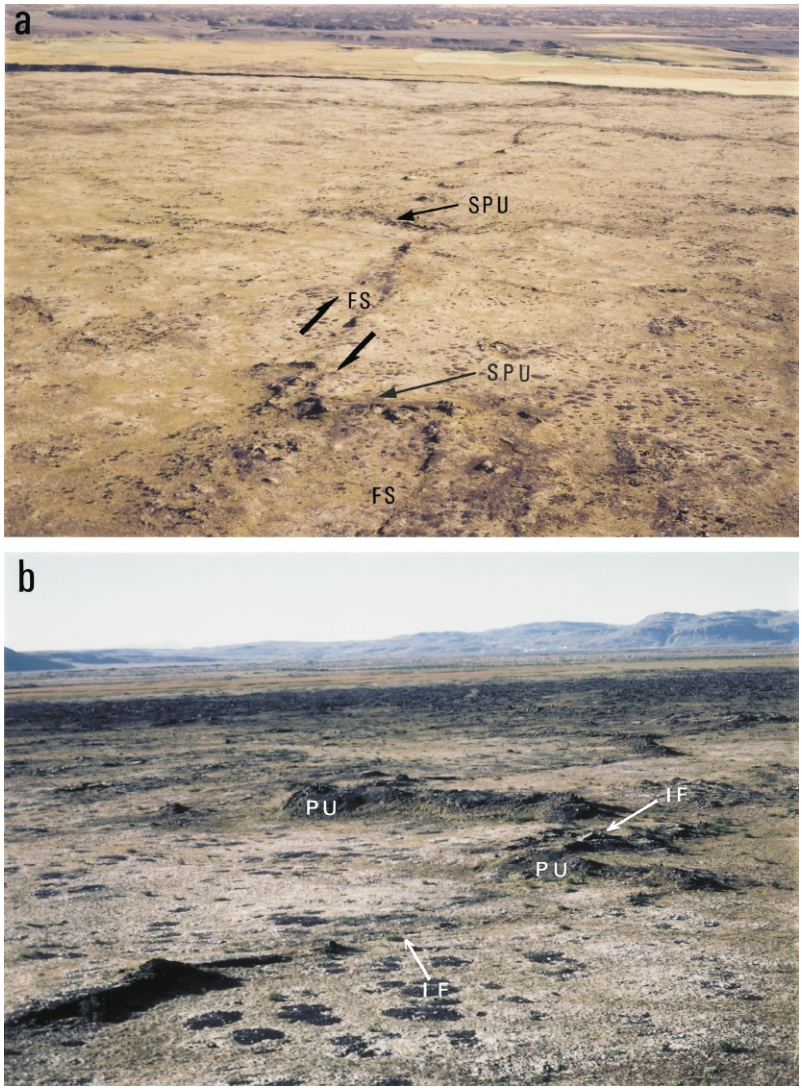

Fig. 5. Aerial photographs of the Leirubakki Fault. (a) Two large sets of push-ups (SPU) at the junction between fault segments (FS). Arrows indicate the right-lateral motion of the fault. (b) Array of fractures with the en-échelon arrangement of individual fractures (IF) and individual push-ups (PU).

features associated with the Leirubakki Fault in great detail in the field (Fig. 7), making numerous additional measurements using compass, clinometer and a measuring tape. The fractures associated with the fault do not consistently display evidence of simple fault displacement. Instead, these fractures commonly have evidence of vertical offset, dilational opening, and push-up ridge development. Most of these measurements dealt with (1) the vertical offsets along each fracture, (2) the width of particular structures such as open fissures or minor grabens, and (3) the height and shape of the push-ups (Figs. 8b and 9). The latter measurements included the dip angles and the lengths of the multiple slabs of broken flow units (beds) that form the external envelope of each push-up. These lengths were measured across strike, that is, perpendicular to the axes of the push-up structures (Fig. 8a), and can thus make a significant, albeit limited, angle with the slip direction of the whole fault.

The amount of shortening, ΔL, calculated in the direction perpendicular to the push-up axis is given (Fig. 10) by:

$$\Delta L = L_0 - L \tag{1}$$

where L_0 is the ground length between points on opposite edges of the push-up in the direction perpendicular to its axis, and L the horizontal width between the same two points. For instance, with a push-up envelope composed of four broken slabs of widths a, b, c, d and with dip angles α, β, γ, δ (Fig. 8b and c) we have:

$$L_0 = a + b + c + d \tag{2}$$

$$L = a\cos\alpha + b\cos\beta + c\cos\gamma + d\cos\delta \tag{3}$$

The shortening across the push-ups corresponds to the shortening in relays between individual fault segments or individual fractures. The length determination was made along a cross-section perpendicular to the push-up axis (Fig. 8; O–O′), in order to minimise errors. Because the push-up axes trend approximately perpendicular to the

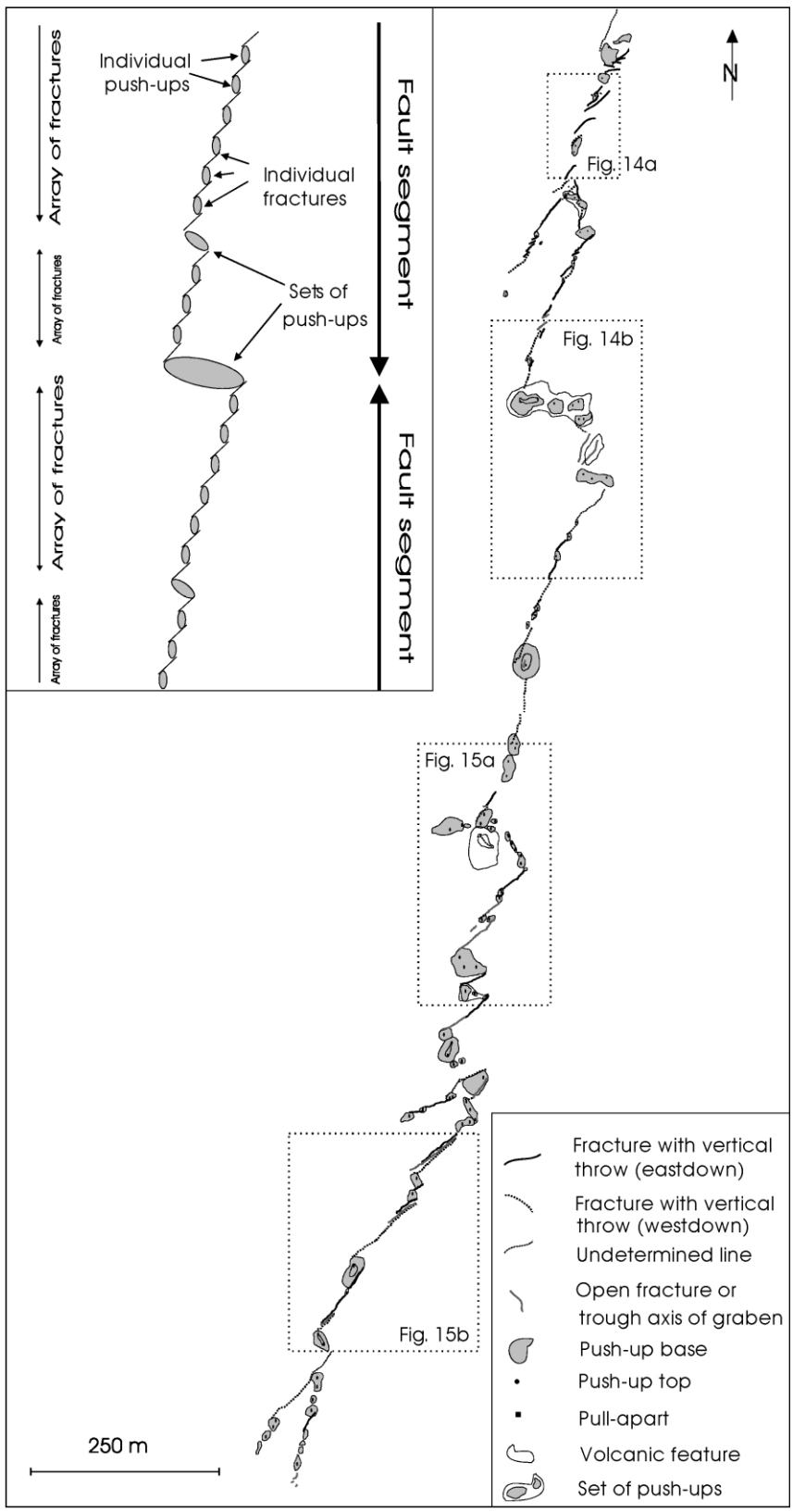

Fig. 6. Map of the central part of the Leirubakki Fault drawn from GPS measurements. The upper inset shows a schematic pattern of the Leirubakki Fault including fault segments and arrays of individual fractures and push-ups. The dotted frames show the location of Figs. 14 and 15.

strike of the individual fault segments or individual fractures, this shortening roughly indicates the slip along the same fault segments or fractures (Fig. 8a). However, for each push-up, we took into account the obliquity between the main fault strike (010°) and the push-up axis trend, in order to re-calculate the shortening measured parallel to the fault, and hence the amount of slip. As Table 1 shows, this correction introduces little difference (see Section 5.1).

In addition to these length measurements, we carried out push-up volume determinations in order to calculate the depth at which the en-échelon pattern is replaced by a single fault (see Section 5.2). In a cross-section perpendicular to the axis of the push-up, the volume per unit length of a push-up is given by the surface area of the section above the base of the push-up, that is, above the level of the surrounding lava flow. Using the same measurements as before (a, b, c, d and α, β, γ, δ in the case of four broken slabs; Fig. 8c), the horizontal and vertical sides of the corresponding triangles are easily calculated. From these values, the across-strike surface area of the push-up section is determined within an assemblage of triangles and rectangles, at the periphery and in the core of the push-up (Fig. 8d). To account for the slight difference in elevation between the two sides of a push-up, it is necessary to add the surface area of a triangle (S_z in Fig. 8d). As shown in Fig. 8d, the volume per unit length of a push-up is finally:

$$S = S_a + S_b + S_c + S_d + S_x + S_y + S_z \quad (4)$$

In these calculations, the base of the push-up must be defined. Because most push-ups are asymmetrical, and because the dip angle of their lowest, peripheral slabs (at least on one side of the push-up) can be very shallow, we generally considered the slope break as the base of the push-up (Fig. 9). There is uncertainty in the case of very shallow dips at the periphery of the push-up, because the surface areas of the corresponding triangles cannot be neglected (Eq. (4)) and may result in a significant additional term when the slabs are large. This uncertainty exists only with volume estimates; when determining shortening (Eqs. (1)–(3) and Fig. 10) the additional term above is negligible (as a consequence of the very shallow slab dip) in comparison with measurement uncertainties. For the volumetric determinations, we solved this problem by measuring the shallow-dipping peripheral portions of the push-up structures.

Another important factor that deserves consideration is the possible presence of voids, as a consequence of the near-surface disruption of the basalt layers, inside the push-ups (Figs. 7c and 10). The surface measured in Fig. 8d, and hence the volume of the push-up structure, is certainly larger than the corresponding surface area and volume before deformation. However, our observations of broken push-ups suggest that the additional volume is generally less than 10%. This extra volume of the initial near-surface disruption is partly compensated for by the subsequent sagging of the push-up structures. Such a gradual reduction in volume of push-ups has been observed after earthquakes in the SISZ (Bjarnason et al., 1993). By ignoring the voids inside a push-up we overestimate the deformed volume, whereas by ignoring the peripheral portions of the push-up we underestimate this volume. Thus, because these sources of uncertainty are similar and act in the opposite sense, the geometrical calculation based on the scheme of Fig. 8 should be regarded correct in first approximation.

4. The rupture trace of the Leirubakki fault

At the surface, the most distinctive feature of the Leirubakki Fault is the en-échelon arrangement of its fractures and push-ups at various scales, characterising a right-lateral strike-slip motion (Fig. 11). This is a common feature of the N–S strike-slip faults of the SISZ (e.g. Bjarnason et al., 1993), but the Leirubakki Fault provides the best large-scale example of this rupture pattern. On a general map drawn from aerial photographs, the Leirubakki Fault can be traced for a length of 7.5 km in the Holocene lava flows, from an area north of the Tjarnalaekur rivulet in the north to an area south of the Ytri Ranga river in the south (Fig. 4). Although the surface of the lava flow is nearly flat over large distances, our detailed mapping revealed a minor difference in elevation in the vicinity of the Leirubakki Fault: the ground surface on the western side of the fault is lower by about 0.4 m, on average, than that on its eastern side. This elevation difference fits with the regional slope of the lava flow. Nevertheless, 52 measurements of vertical displacements along the fault show a larger proportion of down-to-the-east than down-to-the-west offsets (30 vs. 22). The average of the down-to-the-west offsets, however, is 0.55 m compared with 0.43 m for the down-to-the-east offsets. Thus, the Leirubakki Fault may be regarded as a pure strike-slip fault where the minor vertical offsets simply reflect the behaviour of local structures along the fault.

Taken as a whole, the Leirubakki Fault strikes 010°. The fault trace, however, includes at least five distinct segments that trend 015°–020° (FS1–FS5 in Fig. 4). Two of these segments (FS1 and FS2) are located north of the road to Skard and Leirubakki (road no. 26). Two other segments that we studied in detail lie between this road and the Ytri–Ranga river (FS3 and FS4); the southernmost segment (FS5) is south of this river (Fig. 4). The length of each fault segment is 1–2 km.

These fault segments can be subdivided into arrays of individual fractures, which are separated by large sets of aligned push-ups (Fig. 6). The average trend of these arrays makes a clockwise angle of 10°–20° to the overall NNE–SSW strike of the fault segments. Each array of individual fractures ranges from 100 to 250 m in length.

The individual fractures that constitute the arrays range from about 8 to 125 m in length, but 65% of these lengths (41 fractures of a total of 63) fall in the length range 10–40 m (Fig. 12a). Many of these fractures are arranged

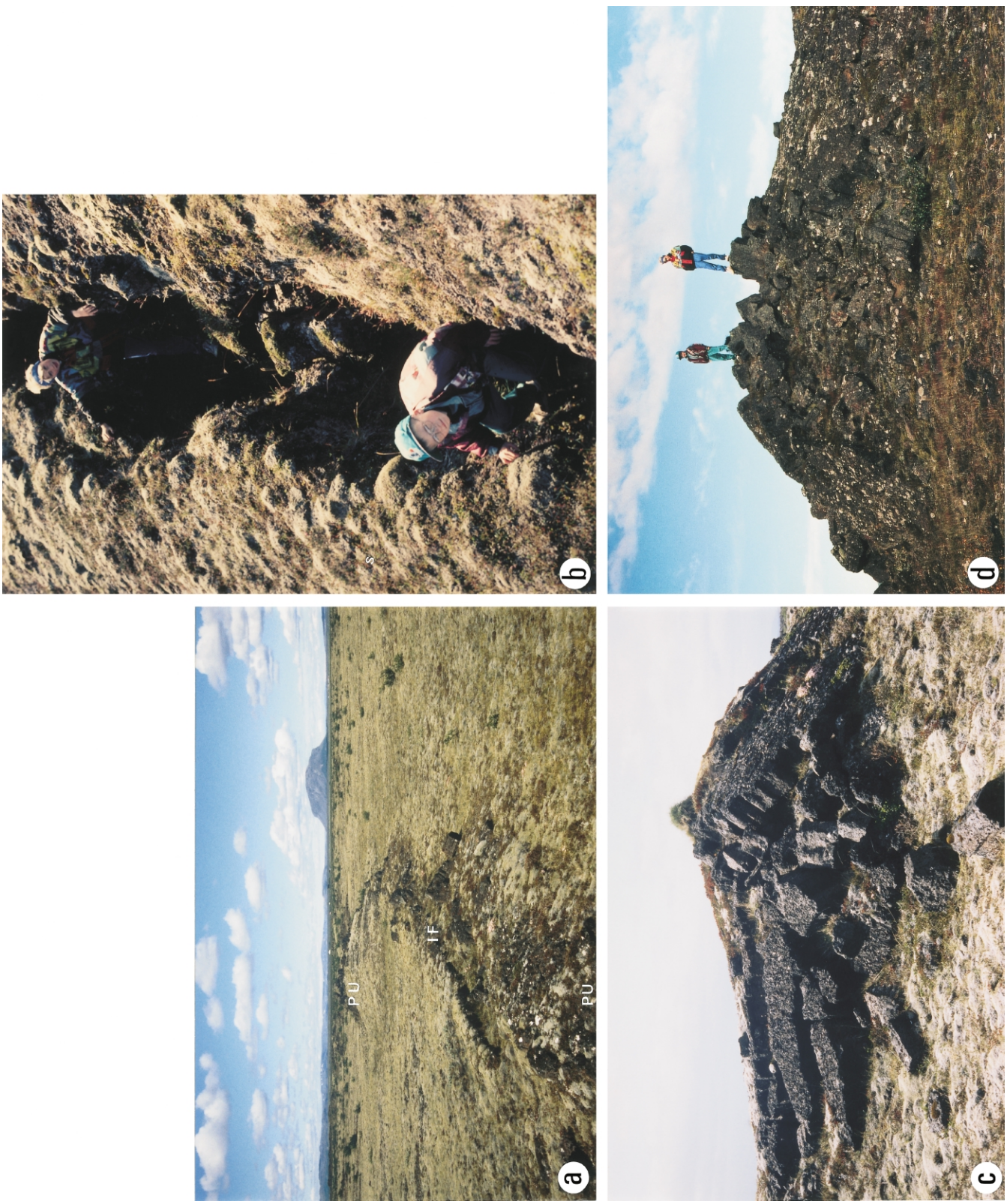
b
S
d
a
PU
IF
PU
c

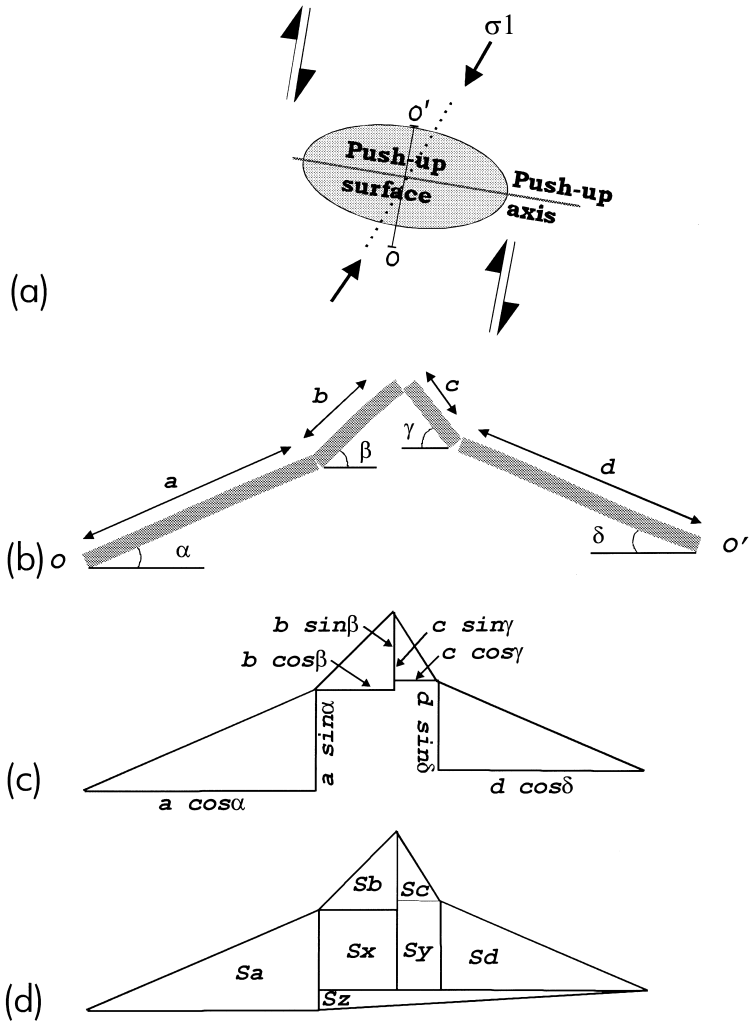

Fig. 8. Schematic representation of a push-up showing the different elements used for slip estimation. (a) Map view. (b) Cross-section. (c) and (d) Elements of calculation. The right-lateral motion of the individual fault segments or individual fractures is indicated, as well as the σ_1 axis corresponding to the regional direction of compression. See text for details of calculations.

en-échelon and separated by push-ups. The average strike of individual fractures is at a clockwise angle of 0°–30° to the trend of the fracture array to which they belong.

The surface rupture of the Leirubakki Fault contains fractures (s.l.) in four size classes which, in decreasing order, are the whole fault system, the fault segments, the arrays of fractures, and the individual fractures. Their lengths range over 3–4 orders of a magnitude, from kilometres to decametres. Also, the azimuthal relationships are similar for fractures in all the size classes (except the largest one) in that the fractures are arranged (clockwise) en échelon relative to the higher-order system that contains them.

The en-échelon arrangement of the fracture segments at various scales accounts for the widely different trends seen on the aerial photographs (Fig. 4), on the GPS-based map (Fig. 6), and in the field. These angular relationships imply that the angle between the individual fractures and the trend of the fault segment to which they belong is never less than 10° nor greater than 50°. Because the fault segments themselves make an angle of 5°–10° to the general trend of the Leirubakki Fault, individual fractures are expected to make angles between 15° and 60° to the main fault. In fact, most angles between individual fractures and fault segments are 10–35°, whereas those between fractures and the whole fault trace are 10–45°. Around 60% of individual fractures range in strike between 030° and 060° (Fig. 12b). These systematic obliquity and en échelon arrangements should be regarded as characteristic of the fault.

Fig. 7. Photographs of some characteristic features along the Leirubakki Fault. (a) Example of an arrangement of push-ups (PU) and individual fractures (IF) forming part of an array of fractures. (b) Example of individual open fracture. (c) Example of a disrupted push-up (H_{max} = 2.3 m). Note the presence of internal voids. (d) The highest push-up within the studied part of the Leirubakki Fault (H_{max} = 4.35 m). This push-up is located in a set of large push-ups at the junction between two main fault segments (see Fig. 14b).

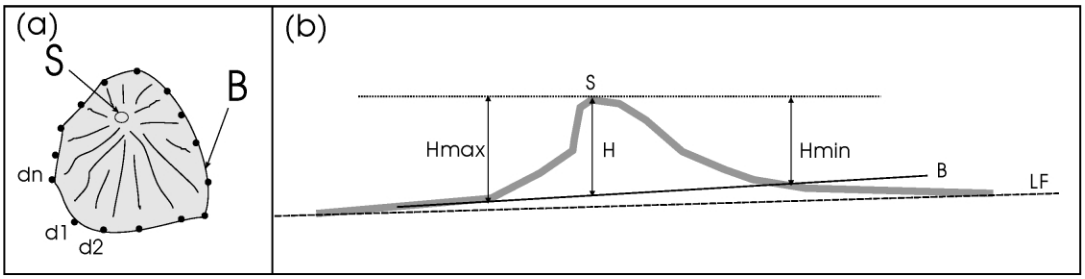

Fig. 9. Schematic representation of a push-up showing the elements used for height estimation. (a) Map of the push-up; d1, d2,…,d*n*: points recorded by GPS measuring all around the push-up and delineating its base. (b) Cross-section of the push-up; S is summit of the push-up; B as full line is the base of the push-up; LF as dashed line is the average lava flow surface; H_{max} and H_{min} represent maximum and minimum heights of the push-up, respectively; H is average height of the push-up. See text for detailed explanations.

All the individual fractures observed along the Leirubakki Fault are vertical or dip very steeply. The strike-slip displacement is dominant on most of these fractures, based on the presence of push-ups at their tips. Most fractures (85% of the total set), however, show apparent vertical offsets, ranging from 0.2 to 1.1 m (Fig. 12c). The vertical throws to the east and west are comparable in frequency and size, supporting the conclusion that the Leirubakki Fault taken as a whole is a pure strike-slip fault. The remaining fractures (15%) are either open or of an undetermined type.

The heights of the push-ups located along the fracture arrays and those that connect the fracture arrays are generally the same, whereas the heights of the push-ups separating the fault segments are normally greater. The maximum height (Fig. 9) of 63 measured push-ups ranges between 0.35 and 4.35 m (Fig. 13). The heights of all push-ups located between the fault segments exceed 2 m. Because most of the push-ups are asymmetrical, we show both their average and maximum heights (Fig. 13). The maximum height of a push-up, H_{max}, as measured on its steep side (Fig. 9b), is the elevation difference between its summit and the lowest point at its base. The average height of a push-up, H, is the elevation difference between its summit and the average altitude of all the points measured around it (Fig. 9a). The histograms of H_{max} and H differ in shape, with a more gradual decrease of H_{max} towards high values. This difference results partly from the presence of large shallow-dipping slabs at the periphery of the largest push-ups, amplifying the contrast between H_{max} and H.

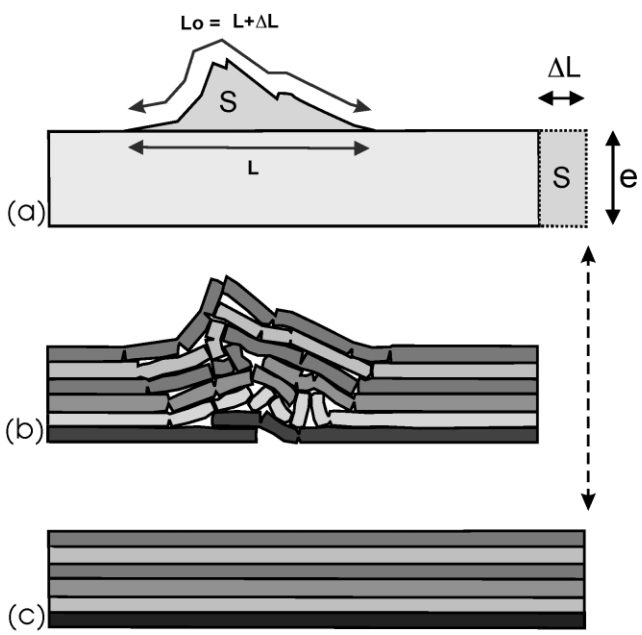

Fig. 10. Schematic cross-section of a push-up. (a) Length between points on opposite edges of the push-up as L_0 and the horizontal width of the same push-up as L; the corresponding slip is $\Delta L = L_0 - L$. The volume per unit length of push-up is given by the surface of the section above the base of the push-up (S), it is used for the evaluation of the depth (e) at which the en-échelon pattern is replaced by a single fault (see Fig. 17). (b) Near-surface disruption of the basalt layers. (c) Aspect of the same basalt layers before push-up formation. See text for explanation.

To illustrate the structure of the Leirubakki rupture trace, four examples have been selected in its central part (located in Fig. 6). These include a typical array of individual fractures and individual push-ups (Fig. 14a), a junction between two fault segments (Fig. 14b), a junction between two arrays of fractures (Fig. 15a), and a typical array of minor grabens (Fig. 15b). Note that any push-up height mentioned for these examples refers to H_{max}.

The first example shows a standard arrangement of push-ups and individual fractures, forming a part of an array of fractures; the fractures trend 035°–055° and are 15–60 m long (Fig. 14a). Their vertical throws average 0.5 m, the downthrown block being either to the west or to the east. Individual fractures trend at 25° to the direction of the fault segment, and at 35° to the general direction of the Leirubakki Fault. The heights of the individual push-ups, from 0.95 to 1.90 m, are similar to those along the whole fault (Fig. 13).

At the junction between two main fault segments, there is a clear 100° alignment of large push-ups (SPU in Fig. 14b), ranging in height from 2 to 4.35 m. The individual push-ups located along the fault segments themselves range in height between 0.70 and 1.60 m. A small pull-apart (PA in Fig. 14b), associated with the southern fault segment, is one of only two such structures among the 70 push-ups and pressure ridges along the studied part of the Leirubakki Fault. A small volcanic depression (VD in Fig. 14b) is also present in the large push-up zone referred to as SPU; such

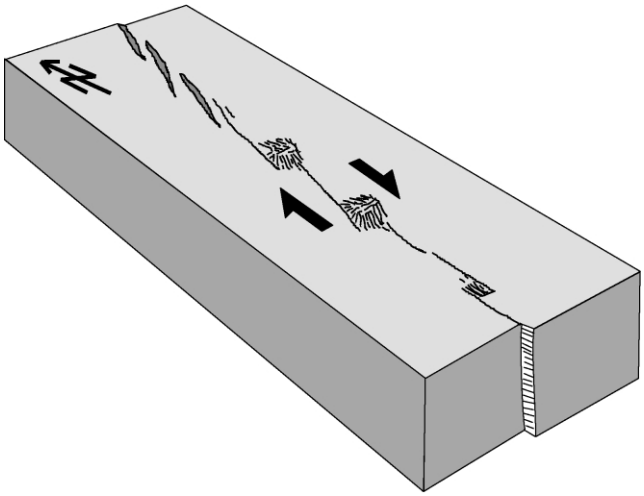

Fig. 11. Schematic field sketch of a right-lateral fault segment showing en-échelon open fractures, strike-slip segments with minor component of dilation, push-up and pull-apart structures (after Bergerat and Angelier, 2000). Arrows indicate the sense of motion consistent with the en-échelon fracture pattern.

volcanic depressions or highs develop during the emplacement of the lava flow, predate faulting and have no tectonic significance.

Fig. 15a shows the junction area between two arrays of fractures. Apart from difference in scale, this junction resembles the one between two fault segments (Fig. 14b), with a series of push-ups in between. Most push-ups range in height between 0.35 and 1.50 m (the same range as for the push-ups connecting the individual fractures), although two push-ups reach the height of 2.35 m. A pre-existing volcanic depression is also present in this area (VD in Fig. 15a). Volcanic depressions exist in zones of multiple push-ups between fault segments (Fig. 14a), or between arrays of fractures (Fig. 15a), probably because they presented pre-existing weaknesses that concentrated stresses and tended to capture the near-surface rupture propagation during fault slip.

Fig. 15b illustrates a typical array of fault-parallel grabens that connect individual push-ups. These grabens, with an average strike of N50°E, make an angle of 40° to the general direction of the Leirubakki Fault. The individual push-ups range between 0.50 and 2.55 m in height, most of them being about 1.50 m. The fractures bounding the northern graben of Fig. 15b dip very steeply and display vertical offsets, to the west and east, of 0.4–0.5 m. The largest vertical offset is 0.8 m, on the eastern edge of the southern graben of Fig. 15b.

5. Length and slip of the Leirubakki Fault

5.1. Displacement estimates

Is the Leirubakki rupture due to a single large earthquake? Because most faults are not monogenic, this cannot be a priori considered certain. However, the surface rupture

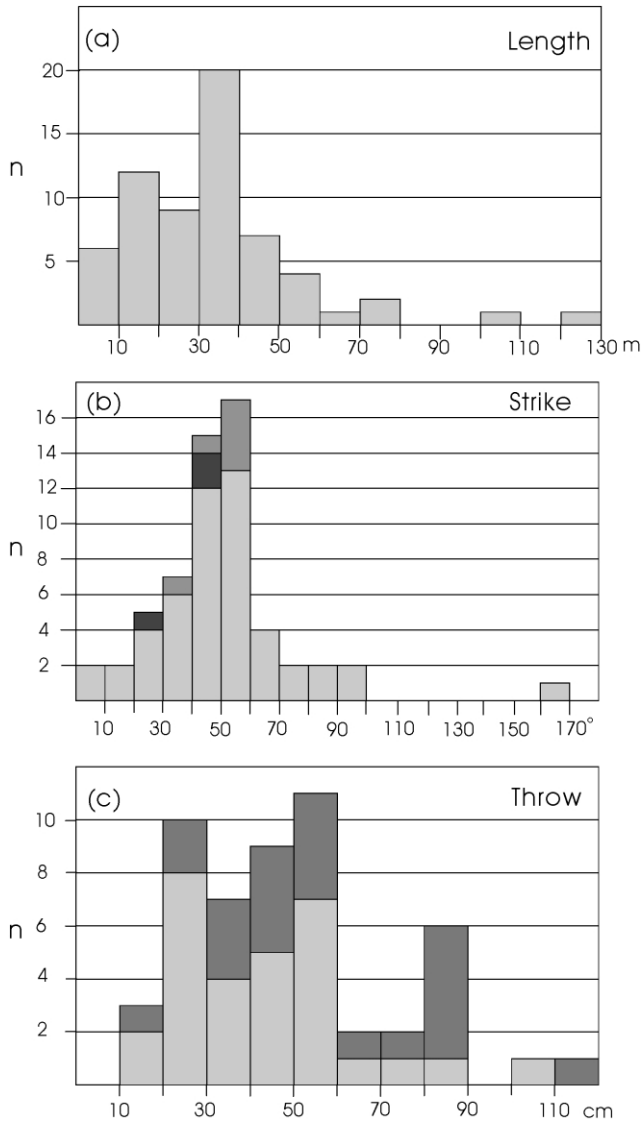

Fig. 12. Characteristics of the individual fractures. (a) Histogram of the fracture lengths. (b) Histogram of the fracture azimuths. Light grey = fractures with a vertical offset, dark grey = open fractures, black = undetermined fractures. (c) Histogram of fracture vertical throws. Light grey = east-throws, dark grey = west-throws; n = number of fractures.

pattern of the Leirubakki Fault as observed in the Holocene lava flow appears to be related to a single large event. The surface structures are very similar to those generated during the M7 1912 event (Selsund Fault; e.g. Bjarnason et al., 1993) as well as the M6.6 June 2000 events (Arnes Fault and Hestfjall Fault; e.g. Bergerat and Angelier, 2001). Furthermore, from the mechanical point of view, simple 4-m-high push-ups (Figs. 5 and 7d) would be very unlikely to be generated by a succession of small events. For these two reasons, we consider that the surface features analysed along the Leirubakki Fault have been created during a single event. This consideration does not introduce any difference concerning the finite displacement estimates, but is crucial for magnitude determination.

Considerations of the shapes and dimensions of push-ups

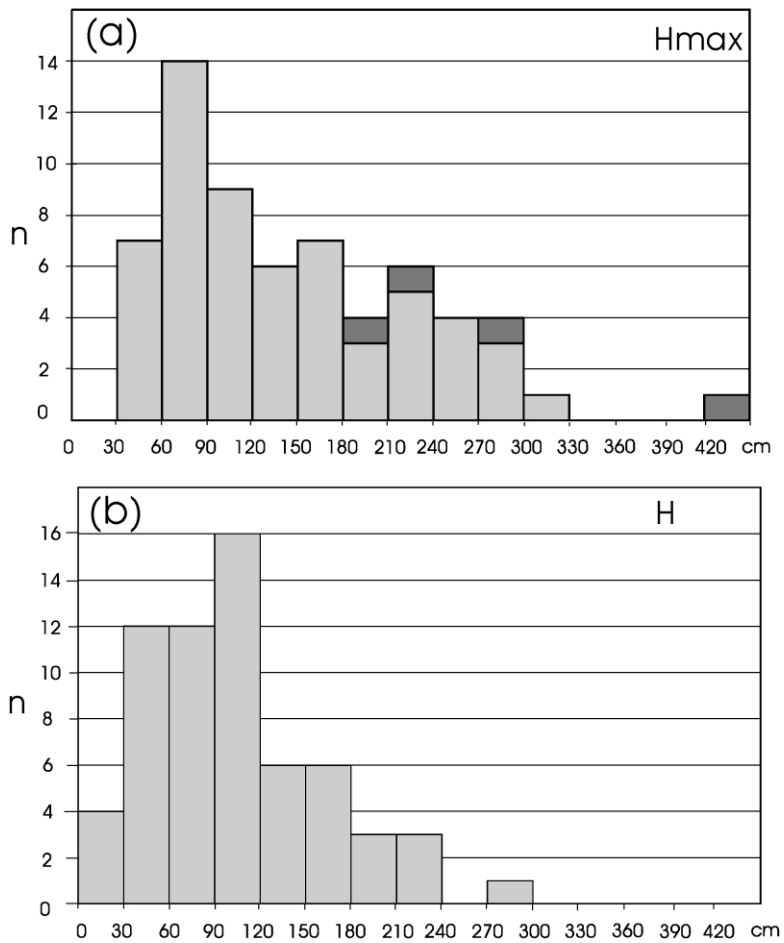

Fig. 13. Characteristics of the push-ups. (a) Histogram of the maximum height of the push-ups (H_{max}). In dark grey are indicated the push-ups located at the junction of the two main fault segments (see Fig. 14b). (b) Histogram of the average height of the push-ups (H) computed from the difference between the altitude of the summit of each push-up and of the average altitude of its base (see Fig. 9).

allowed us to determine the fault displacement at 15 locations. These determinations were made in the direction perpendicular to each push-up axis. One example is presented in Fig. 16, and all results are given in Table 1. Among the 15 push-up structures where detailed cross-sections were made, four accommodate only a limited proportion of the fault displacement, so that the corresponding estimates (0.23–0.96 m, 0.65 m on average) should be regarded as very low values. In four other cases, this proportion is larger than 50%, and the amounts of shortening range from 1.15 to 2.16 m (1.54 m on average). Four push-ups form two couples, each couple accommodating most of the displacement (1.37 and 1.58 m). Each of the remaining three push-ups accommodates nearly the total displacement, with values from 1.36 to 2.67 m (1.88 m on average).

The displacements measured in the central part of the Leirubakki Fault range from 0.23 to 2.67 m, with a mean value of 1.13 m (Table 1). This mean value, however, does not necessarily represent the average fault displacement for three reasons. First, the uncertainties in the displacement determinations may vary. Second, the distribution of

Table 1
Estimation of the displacement along the Leirubakki Fault (LF). From left to right: values of displacement for each measured push-up, trend perpendicular to the push-up axis (O–O′ in Fig. 8) (GN: Geographic North) and values of the displacement along the Leirubakki Fault. Last line: average (AD and AD_L) and maximum (MD and MD_L) displacements

Displacement D_A	Trend of O–O′ (/GN) α_A	Displacement along LF D_L
0.24	032	0.22
1.36	177	1.32
0.53	152	0.42
0.84	172	0.80
1.33	097	0.07
1.26	097	0.06
0.75	007	0.75
0.96	032	0.89
2.67	044	2.21
0.23	017	0.23
0.40	017	0.39
1.62	017	1.60
2.16	017	2.14
1.53	022	1.49
1.15	024	1.11
AD/MD		AD_L/MD_L along LF
1.13/2.67		0.91/2.21

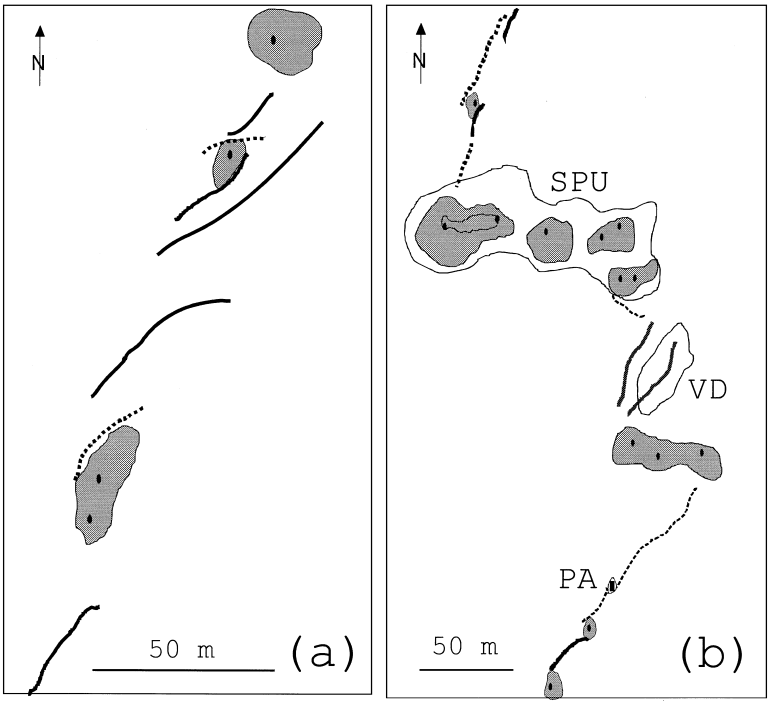

Fig. 14. Detailed parts of the Leirubakki Fault map showing (a) a typical array of individual fractures and individual push-ups and (b) the junction between two fault segments. Legend as for Fig. 6.

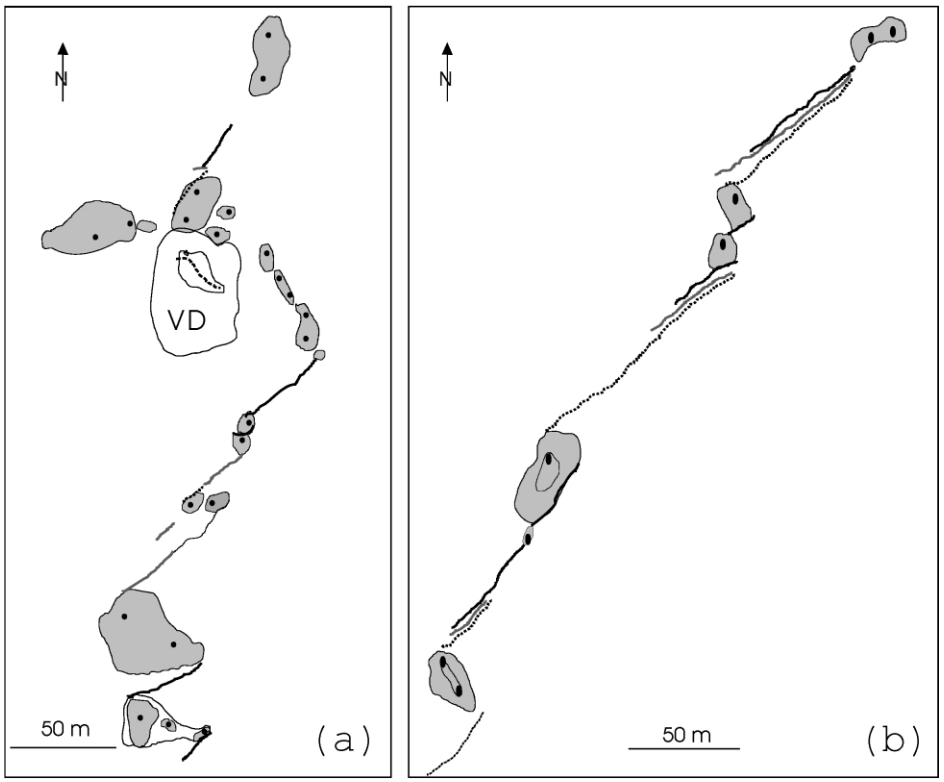

Fig. 15. Detailed part of the Leirubakki Fault map showing (a) the junction between two arrays of fractures and (b) a typical array of grabens. Legend as for Fig. 6.

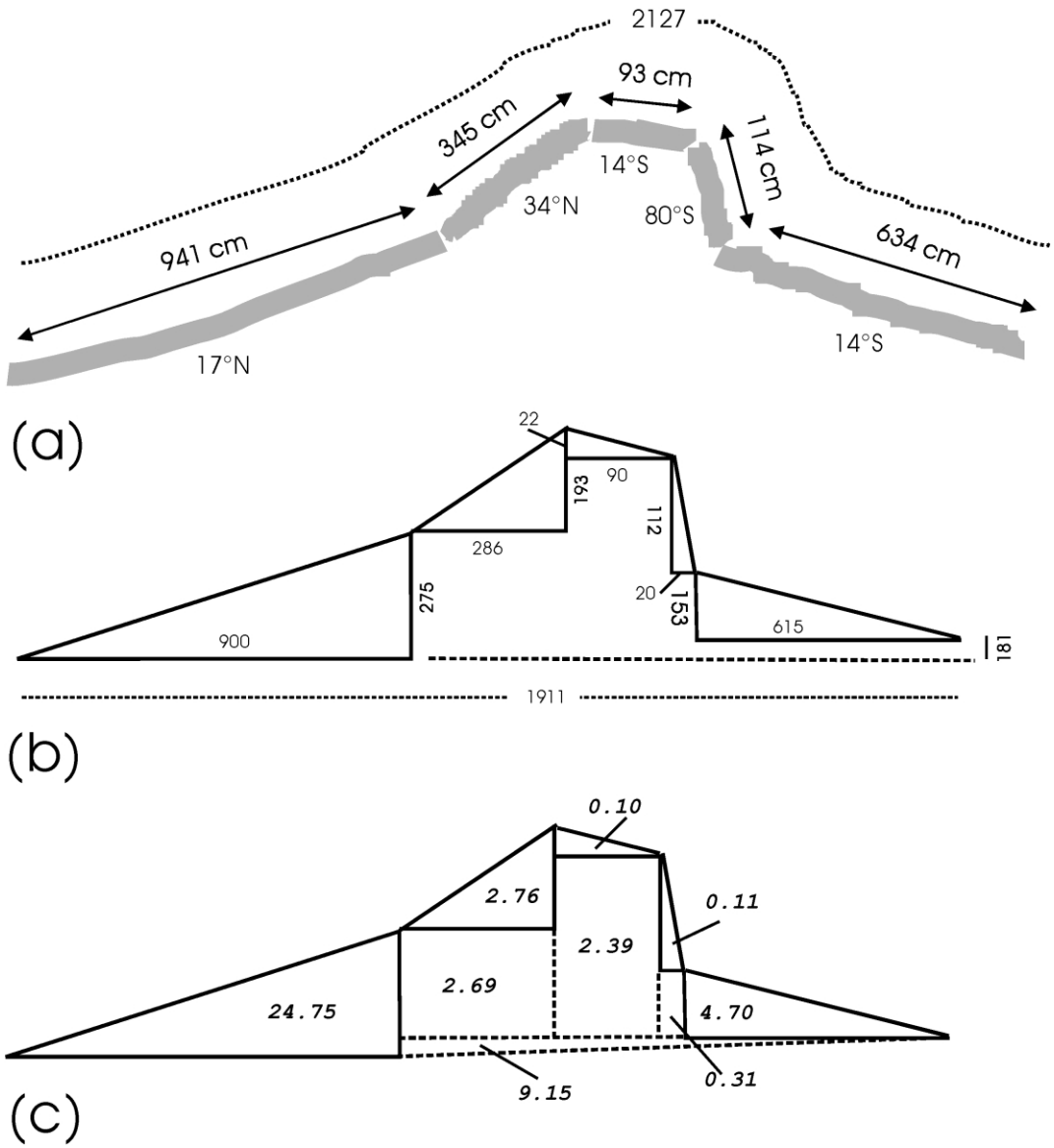

Fig. 16. Calculation of the dimensions of a characteristic push-up as example. (a) Widths and dip angles of the multiple slabs of broken flow beds that form the external envelope of the push-up. (b) Calculation of the horizontal and vertical sides of the corresponding triangles. (c) Determination of the across-strike surface of the push-up section within an assemblage of triangles and rectangles. The computed elements are used to evaluate the displacements in the direction perpendicular to the push-up axis (see Fig. 8 and Table 1) and the depth at which the en-échelon pattern is replaced by a single fault (see Fig. 10).

the displacement–determination sites along the fault is not uniform. Third, some of the determinations yield only a fraction of the displacement, especially where the fault splits into branches so that a significant amount of displacement may be accommodated on a subsidiary fault segment (Figs. 4 and 6). Note also that whereas most push-up axes trend almost perpendicular to the fault direction (Fig. 8a), a few similar structures trend oblique at small angles to the fault direction and thus should be regarded as pressure ridges rather than push-ups. For these reasons, the shortening values that best account for the displacement of the Leirubakki Fault are those obtained for the largest push-up structures elongated in a direction perpendicular to the fault trend. We consequently emphasise the largest displacements in the calculations presented in Section 6.

Because the displacement estimates were made along the direction perpendicular to the axis of each push-up structure, which may be slightly oblique to the general trend of the Leirubakki Fault, for a more rigorous calculation the following correction is used:

$$D_L = D_A \times \cos(\alpha_A - \alpha_L) \quad (5)$$

where D_A is the measured displacement, D_L the amount of slip of the Leirubakki Fault, and $(\alpha_A - \alpha_L)$ the difference between the direction perpendicular to the push-up axis and the 010° trend of the Leirubakki Fault (Table 1).

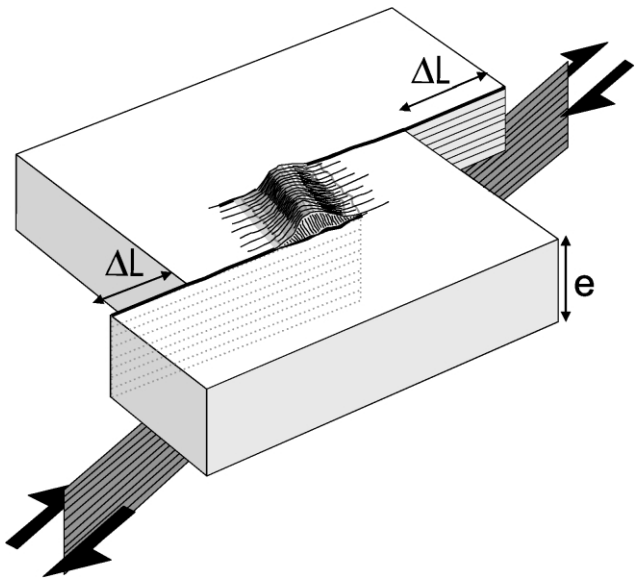

Fig. 17. Schematic view of a push-up and en-échelon fractures in the uppermost part of the crust and a single right-lateral strike-slip fault at depth. As for Fig. 10, ΔL is the slip calculated from the push-up dimensions and e the depth at which the en-échelon pattern is replaced by a single fault.

5.2. Depth estimates

The en-échelon arrays of individual fractures constituting the different fault segments of the Leirubakki Fault form a pattern typical for a single strike-slip fault (e.g. Riedel, 1929; Tchalenko and Ambraseys, 1970; Gamond and Giraud, 1982; Etchecopar et al., 1986; Bellardinelli et al., 2000). Fig. 17 illustrates the relationships between a push-up associated with en-échelon fractures at the surface and the single fault at depth. The depth, e, at which the en-échelon pattern is replaced by a single fault can be calculated as a function of both the amount of shortening, ΔL, and the volume per unit length of push-up, S, as follows (Fig. 10):

$$e = S/\Delta L \tag{6}$$

The calculations have been made for 14 push-ups (Table 2) where we could perform reliable measurements of ΔL (as shown in Figs. 8b and 10) and S (as shown in Fig. 8d). Before determining the values of e, it is worth noting that these push-ups correspond to different positions in the Leirubakki fault pattern. Four push-ups reflect a local behaviour of the uppermost lava beds, as confirmed by the low values of e in three cases (2.6–2.9 m). For the remaining 11 push-ups, the values of e obtained range between 5.1 and 33 m, giving an average value of 14.8 m. In more detail, the distribution of these values is bimodal, with average values of 7.4 m (six values in the range 5.1–12.8 m) and 23.6 m (five values in the range 16.1–33.0 m). Interestingly, the push-ups corresponding to each range of values are not scattered along the fault but belong to few spatial groups. Our determinations indicate that the push-up structures are rooted at two main levels, at depths of about 7.4 and 23.6 m below the lava flow surface, which may correspond to two basalt flow units.

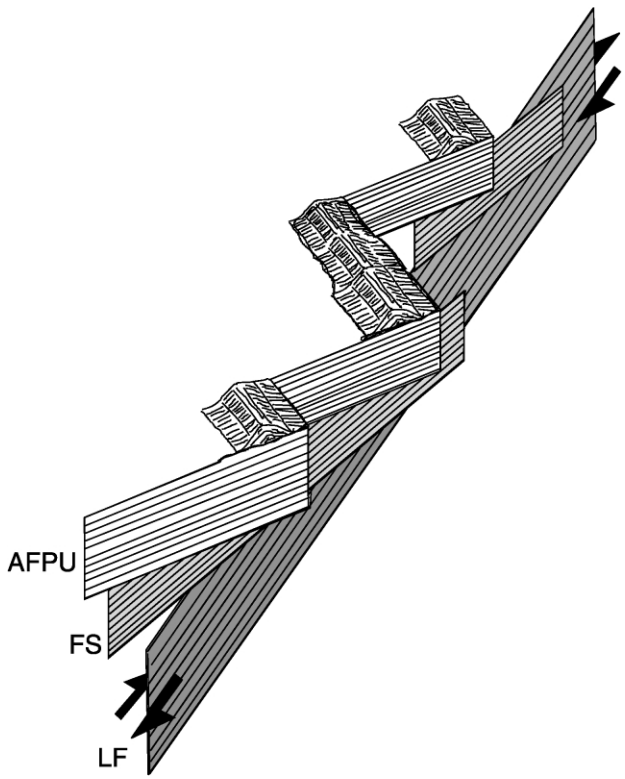

Fig. 18. Schematic sketch of the superposition of en-échelon systems of faults in depth. From top to bottom: the en-échelon arrays of fractures and push-ups (AFPU), the en-échelon deep faults corresponding to the different fault segments (FS) and the main Leirubakki Fault plane (LF).

We conclude that the transitions between the fault systems at different levels may relate to the presence of local décollements between the main basalt layers. This

Table 2
Estimation of the depth at which the en-échelon pattern is replaced by a single fault. From left to right: amount of shortening ΔL, volume per unit length of push-up S and estimation of the single fault depth e

ΔL (m)	S (m^2)	e (m)
1.53	50.55	33.04
2.16	46.96	21.74
0.75	64.51	86
1.15	20.43	17.76
0.84	5.91	7.03
0.24	0.7	2.91
1.36	17.45	12.83
0.53	2.67	5.05
1.33	8.70	6.54
1.26	7.20	5.72
0.96	15.64	16.3
2.67	7.80	29.2
1.62	11.62	7.17
0.32	0.83	2.6

interpretation is also supported by the location of the deepest e values (around 23.6 m) along the fault segments, whereas the shallowest e values (around 7.4 m) are found in the junction zones between fault segments, in agreement with the strike-slip fault arrangement suggested in Figs. 17 and 18. As pointed out earlier, the arrays of fractures are arranged en-échelon along the fault segments and the fault segments themselves are arranged en-échelon along the Leirubakki fault (Figs. 4 and 6). As a consequence, it is very likely that the deepest fault shown in Fig. 17 also belongs to an en-échelon system, which probably reflects dextral slip on a deeper and larger fault, as depicted in Fig. 18.

6. Magnitude of the Leirubakki earthquake

Based on a compilation of a world-wide historical database of 244 earthquakes, Wells and Coppersmith (1994) presented empirical relationships between various parameters such as the moment magnitude, the surface and subsurface rupture lengths, the down-dip rupture width, the rupture area, the maximum and average displacements. In particular, the log-linear regressions between earthquake magnitudes and surface rupture lengths showed good correlation. For magnitude and displacement and displacement and rupture length, the correlation was poorer and the standard deviation larger. There was no significant difference between data from compressional and extensional regimes, suggesting that the regression laws do not depend much on the tectonic setting. Because we could determine both the length and the displacement of the Leirubakki Fault, it is possible to estimate the magnitude of the Leirubakki earthquake based on such regression laws.

The major source of uncertainty is the length of the rupture trace because it is difficult to follow it in the aa lava flows. Discontinuous surface fractures at each end of the main, and well-exposed, surface trace are here considered parts of the tectonic surface rupture and included in the calculations. The minimum length of the fault, based on the field observations and the aerial survey, is 7.5 km, but it is likely to be much longer as both lateral ends are uncertain.

Knowing the actual slip vector of the Leirubakki Fault, we use the coefficients for strike-slip faulting given by Wells and Coppersmith (1994). The moment magnitude (M) as a function of the decimal logarithm of the surface rupture length (SRL) of the fault is given by:

$$M = 5.16 + 1.12 \times \log_{10}(\mathrm{SRL}) \quad (7)$$

For the Leirubakki Fault, with SRL = 7.5 km, we obtain $M = 6.14$.

As indicated above, the surface rupture trace length, 7.5 km, is likely to be much less than the true surface length of the Leirubakki Fault. This conclusion is supported by considerations of the Selsund 1912 earthquake rupture (Bjarnason et al., 1993). There the mapped length of the currently observable surface trace is only 9 km, which, according to Eq. (7), corresponds to a magnitude 6.2 earthquake, whereas the actual instrumental magnitude of this earthquake is 7. Observations made just after the 1912 rupture indicate an actual length of at least 20 km (Bjarnason et al., 1993). The southern part of the Selsund Fault is covered by sand or located in aa lava flows, which is also the case for the end segments of the Leirubakki Fault. Some authors infer the total length of the 1912 surface rupture to be 32 km (Stefánsson et al., 1999), and Eq. (7) would give 44 km. Moreover, the June 2000 earthquakes in the SISZ fit the empirical relationship of Eq. (7). For the 17 June 2000 fault, based on the 6.5 moment magnitude, we obtain a length of 16 km, which is exactly the length of the fault as defined by the alignment of aftershocks (Stefánsson et al., 2000), and less than the 20 km length of the surface trace of the fault. Because the length of the Leirubakki rupture trace is probably underestimated, the moment magnitude inferred above ($M = 6.14$) should be considered as a minimum.

Another regression law, giving the earthquake magnitude as a function of the size of fault displacement, can be used to determine the magnitude of the Leirubakki earthquake. For the central part of the Leirubakki Fault, we quantified the fault displacement, based on measurements of the observed push-ups, as being between 0.23 and 2.67 m, with an average of 1.13 m (Table 1). The relationships between the moment magnitude M and the maximum (MD) and average (AD) displacements (in metres) are (Wells and Coppersmith, 1994):

$$M = 6.81 + 0.78 \times \log_{10}(MD) \quad (8)$$

$$M = 7.04 + 0.89 \times \log_{10}(AD) \quad (9)$$

For $AD = 1.13$ m, the magnitude of the Leirubakki earthquake is 7.09, but for $MD = 2.67$ m the magnitude is 7.14.

Adopting the corrected values of displacements (based on the general trend of the Leirubakki Fault; see Table 1), $MD = 2.21$ m and $AD = 0.91$ m, Eqs. (8) and (9) yield moment magnitudes of 7.07 and 7.0, respectively. Thus, the corrected displacement values yield earthquake magnitudes very similar to those obtained from the uncorrected values (MD gives $M = 7.07–7.14$ and AD gives $M = 7.0–7.09$), and, as indicated above, most displacements based on the push-up structures are probably underestimates. Based on these results, we conclude that the moment magnitude of the Leirubakki earthquake was around 7.1.

If this magnitude estimate is correct, it follows from Eq. (6) that the total surface length of the Leirubakki Fault is about 54 km. This is much greater than the mapped length (less than 10 km) but consistent with the corrected length of the fault trace of the Selsund 1912 earthquake.

Using earthquakes from the Eastern Mediterranean region, Ambraseys and Jackson (1998) obtained linear relationships between the surface-wave magnitude M_s and

SRL (in kilometres) and *MD* (in centimetres) in the form:

$$M_s = 5.27 + 1.14 \times \log_{10}(\mathrm{SRL}) \quad (10)$$

$$M_s = 5.21 + 0.78 \times \log(MD) \quad (11)$$

and non-linear relations in the form:

$$M_s = 5.06 + 1.42 \times \log(\mathrm{SRL}) - 0.14[\log(\mathrm{SRL})]^2 \quad (12)$$

$$M_s = 5.11 + 0.86 \times \log(\mathrm{SRL}) + 0.21 \times \log(MD) \quad (13)$$

Applying these equations to the Leirubakki Fault, with SRL = 7.5 km and $MD = 221$ cm, we obtain $M_s = 6.26$ (Eq. (10)), $M_s = 7.03$ (Eq. (11)), $M_s = 6.22$ (Eq. (12)) and $M_s = 6.35$ (Eq. (13)). We have inferred that the measured length of the Leirubakki surface rupture is an underestimate and that the maximum displacement is the most accurate measure of the earthquake magnitude. Then, from Eq. (11), we obtain the magnitude of 7.03, a value close to the value 7.14 calculated from Eq. (8).

Ambraseys and Jackson also proposed an empirical equation to compute the total length of the fault from the magnitude of the associated earthquake, in the form:

$$\log_{10}(\mathrm{SRL}) = -4.09 + 0.82M \quad (14)$$

Applying this equation to the Leirubakki Fault, we obtain a length of 47 km, close to the value of 54 km given by Eq. (7).

7. Conclusion

General mapping based on aerial photographs of the 010°-trending right-lateral Leirubakki Fault, as well as field measurements and GPS mapping conducted along well exposed surface traces in the Holocene lava field, allowed us to identify the main features of the entire fault trace. The surface rupture contains fractures that range in four size classes, over four orders of a magnitude from kilometres to decametres. They are in decreasing order: the main fault, the fault segments, the fracture arrays, and the individual fractures. The features of the three last scalar systems are arranged en échelon (clockwise), relative to the higher-order system that contains them. All these systems correspond to a single large fault at depth.

Detailed measurements made on some push-ups yielded a value of 2.67 m for the maximum right-lateral displacement on the studied part of the Leirubakki Fault. Using empirical relationships established globally, it is proposed that the true rupture length of the Leirubakki Fault is around 50 km and that it gave rise to an earthquake of a moment magnitude 7.1.

Our study of the Leirubakki Fault complements other studies of major historical earthquake faults in the SISZ (e.g. Einarsson et al., 1981; Einarsson and Eiriksson, 1982a, b; Bjarnason et al., 1993), as well as other structural studies including analyses of aerial photographs, local observations of major faults, and collection of minor fault slip data (Passerini et al., 1990, 1997; Gudmundsson and Brynjolfsson, 1993; Luxey et al., 1997; Bergerat et al., 1998, 1999; Bergerat and Angelier, 2000). The trend of regional fractures in the Pleistocene and Holocene rocks of the SISZ ranges from N–S to ENE–WSW, with three main peaks. One peak is at 030°–045°, where most of the fractures are normal faults. Another peak is at 000°–020°, most of the fractures being right-lateral strike-slip faults. The third peak is at 050°–080°, where most of the fractures are left-lateral strike-slip faults (Gudmundsson, 1995; Bergerat et al., 1999; Bergerat and Angelier, 2000).

One of the main characteristics of the seismogenic faulting in the SISZ during historical times is the presence of N–S-trending major earthquake fault traces, such as the faults at Selsund and Leirubakki. In the Holocene lava flows, these N–S faults are much more conspicuous than the ENE–WSW left-lateral strike-slip faults. Current focal mechanisms of microearthquakes ($1 < M < 2.6$) indicate as well that slip on the N–S right-lateral faults may be more common than slip on the ENE–WSW left-lateral faults (Rögnvaldsson and Slunga, 1994).

The crucial question is: why does shearing occur on N–S faults? In ordinary settings, the state of stress in the SISZ (NW–SE extension and NE–SW compression; see Angelier et al., 1996; Bergerat et al., 1998) and the left-lateral transform-type deformation would favour development of, and sliding on, an incipient system of left-lateral en-échelon faults at angles of about 30° relative to the SISZ, the conjugate dextral faults being smaller and less numerous because of the overall sinistral shear. For a mature transform fault zone, this fracture pattern would evolve into a system of major, transform-parallel, left-lateral faults. However, the inherited structural trends in the present-day SISZ are those of the rift zones (NE–SW trending normal faults; cf. Fig. 2). Because of the convenient orientation of these surfaces of weakness relative to the subsequent stress, the shear reactivation of these faults would have been mechanically easier than rupturing and the creation of new faults. The SISZ, however, is not a typical and simple transform zone and has many characteristics of a region between overlapping spreading centres (e.g. Morgan and Kleinrock, 1991; Gudmundsson, 1995, 2000).

We tentatively propose that the SISZ may represent a weak zone with a relatively high thermal flow related to the neighbouring apex of the Icelandic ‘hot spot’ (Fig. 1). This zone would behave at depth like a narrow E–W-trending stripe with thermal–rheological properties that allow development of N–S-trending structures (possibly dyke intrusions) propagating into the seismogenic crust about 10 km thick. According to this interpretation, the scarcity of clear expression of left-lateral strike-slip faulting in the thin brittle crust is related to the distribution of the shear stress across a zone with a quite significant width. In other words, the E–W left-lateral slip is still essentially accommodated in the young and hot lithosphere by pervasive shear deformation across a rather wide zone, so that discrete

left-lateral faulting is expected to develop at a future stage in a cooler crust subject to increasing displacement.

Acknowledgments

Financial support was provided by the European Commission (contract ENV4-CT97-0536), by the IFRTP (Arctic Program 316), and by the French–Icelandic scientific–cultural collaboration program (Iceland Ministry of Education and Culture and French Ministère des Affaires Etrangères). We thank the French Embassy in Iceland for its help, and Richard J. Norris, Páll Einarsson, and David A. Ferrill for constructive reviews.

References

Ambraseys, N.N., Jackson, J.A., 1998. Faulting associated with historical and recent earthquakes in the eastern Mediterranean region. Geophysical Journal International 133, 390–406.

Angelier, J., Rögnvaldsson, S.Th., Bergerat, F., Gudmundsson, A., Jakobsdottir, S., Stefansson, R., 1996. Focal mechanisms of earthquakes and recent faulting: a seismotectonic analysis of the Vördufell area, South Iceland Seismic Zone. Proceedings of the XXV^{e} General Assembly of the European Seismological Commission, Reykjavik, pp. 199–204.

Belardinelli, M.E., Bonafede, M., Gudmundsson, A., 2000. Secondary earthquake fractures generated by a strike-slip fault in the South Iceland Seismic Zone. Journal of Geophysical Research 105, 13613–13629.

Bergerat, F., Angelier, J., 2000. The South Iceland Seismic Zone: tectonic and seismotectonic analyses revealing the evolution from rifting to transform motion. Journal of Geodynamics 29, 211–231.

Bergerat, F., Angelier, J., 2001. Mécanismes des failles des séismes des 17 et 21 Juin 2000 dans la Zone Sismique Sud-Islandaise d'après les traces de surface des failles d'Árnes et de l'Hestfjall. Comptes Rendus de l'Académie des Sciences 333, 35–44.

Bergerat, F., Gudmundsson, A., Angelier, J., Rögnvaldsson, S.Th., 1998. Seismotectonics of the central part of the South Iceland Seismic Zone. Tectonophysics 298, 319–335.

Bergerat, F., Angelier, J., Verrier, S., 1999. Tectonic stress regimes, rift extension and transform motion: the South Iceland Seismic Zone. Geodinamica Acta 12, 303–319.

Bjarnason, I.Th., Cowie, P., Anders, M.H., Seeber, L., Scholz, C.H., 1993. The 1912 Iceland earthquake rupture: growth and development of a nascent transform system. Bulletin of the Seismological Society of America 83, 416–435.

Björnsson, S., 1975. Earthquakes in Iceland. Náttúrufraedingurinn 45, 110–133.(in Icelandic with English abstract).

Björnsson, S., 1978. Large Earthquakes in South Iceland. In: Report of Working Group to the Civil Defence of Iceland, Reykjavik (in Icelandic).

DeMets, C., Gordon, R.G., Argus, F., Stein, S., 1990. Current plate motions. Geophysical Journal International 101, 425–478.

DeMets, C., Gordon, R.G., Argus, F., Stein, S., 1994. Effect of recent revisions to the geomagnetic reversal time scale on estimates of current plate motions. Geophysical Research Letters 21, 2191–2194.

Einarsson, P., 1991. Earthquakes and present-day tectonism in Iceland. Tectonophysics 189, 261–279.

Einarsson, P., Björnsson, S., 1979. Earthquakes in Iceland. Jökull 29, 37–43.

Einarsson, P., Eiriksson, J., 1982. Jardskjalftasprungur á Landi og Rangarvöllum. In: Eldur er i nordri, Sögufélag, Reykjavik, pp. 295–310.

Einarsson, P., Eiriksson, J., 1982b. Earthquake fractures in the districts Land and Rangárvellir in the south Iceland seismic zone. Jökull 32, 113–120.

Einarsson, P., Björnsson, S., Foulger, G., Stefansson, R., Skaftadottir, Th., 1981. Seismicity pattern in the South Iceland Seismic Zone. In: Simpson, D.W., Richards, P.G. (Eds.), Earthquake Prediction: An International Review, AGU Maurice Ewing Series 4, Washington, DC, pp. 141–151.

Etchecopar, A., Granier, T., Larroque, J.M., 1986. Origine des fentes en échelon: propagation des failles. Comptes Rendus de l'Académie des Sciences 302, 479–484.

Gamond, J.F., Giraud, A., 1982. Identification des zones de faille à l'aide des associations de fractures de second ordre. Bulletin de la Société Géologique de France 24, 755–762.

Gudmundsson, A., 1995. Ocean-ridge discontinuities in Iceland. Journal of the Geological Society 152, 1011–1015.

Gudmundsson, A., 2000. Dynamics of volcanic systems in Iceland: example of tectonism and volcanism at juxtaposed hot spot and mid-ocean ridge systems. Annual Review of Earth and Planetary Sciences 28, 107–140.

Gudmundsson, A., Brynjolfsson, S., 1993. Overlapping rift-zone segments and the evolution of the South Iceland Seismic Zone. Geophysical Research Letters 20, 1903–1906.

Halldorsson, P., Stefansson, R., Einarsson, P., Björnsson, S., 1984. Mat á jardskjálftahættu Dysnes, Geldinganes, Helguvík, Vatnsleysuvík, Vogastapi og Porlakshofn, Stadarvalsnefnd um idnrekstur, Idnadarraduneytid, Reykjavík.

Jóhannesson, H., Jakobsson, S.P., Saedmundsson, K., 1990. Geological map of Iceland, sheet 6, south Iceland. Icelandic Museum of Natural History and Iceland Geodetic Survey, Reykjavik, scale 1:250,000.

Karnik, V., 1969. Seismicity of the European Area, Part I, Reidel, Dordrecht, Holland.

Luxey, P., Blondel, Ph., Parson, L.M., 1997. Tectonic significance of the South Iceland Seismic Transform Zone. Journal of Geophysical Research 102, 17967–17980.

Morgan, J.P., Kleinrock, M.C., 1991. Transform zone migration: implications of bookshelf faulting at oceanic and Icelandic propagating ridges. Tectonics 10, 920–935.

Passerini, P., Sguazzoni, G., Marcucci, M., Zan, L., 1990. Slickensides in Western and Southern Iceland: data from Langavatn, Burfell and Vördufell. Ofioliti 15, 191–196.

Passerini, P., Marcucci, M., Sguazzoni, G., Pecchioni, E., 1997. Longitudinal strike-slip faults in oceanic rifting: a mesostructural study from western to southeastern Iceland. Tectonophysics 269, 65–89.

Riedel, W., 1929. Zur Mechanik geologischer Brucherscheinungen. Zentralblatt für Mineralogie, Geologie und Paläontologie 1929B, 354–368.

Rögnvaldsson, S.Th., Slunga, R., 1994. Single and joint fault plane solutions for microearthquakes in South Iceland. Tectonophysics 237, 73–80.

Saemundsson, K., 1979. Outline of the geology of Iceland. Jökull 29, 7–28.

Stefánsson, R., 1979. Catastrophic earthquakes in Iceland. Tectonophysics 53, 273–278.

Stefánsson, R., Bödvarsson, R., Slunga, R., Einarsson, P., Jakobsdottir, S.S., Bungum, H., Gregersen, S., Havskov, J., Hjelme, J., Korhonen, H., 1993. Earthquake prediction research in the South Iceland Seismic Zone and the SIL project. Bulletin of the Seismological Society of America 83, 696–716.

Stefánsson, R., Bergerat, F., Bonafede, M., Böðvarsson, R., Crampin, S., Feigl, K., Roth, F., Sigmundsson, F., Slunga., R., 1999. Earthquake-Prediction Research in a Natural Laboratory Prenlab-Two. Edited Annual Report. ENV4-0536, Reykjavik.

Stefánsson, R., Gudmundsson, G.B., Halldórsson, P., 2000. The two large

earthquakes in the South Iceland seismic zone on June 17 and 21, 2000. URL: http://vedur.is.

Tchalenko, J.S., Ambraseys, N.N., 1970. Structural analysis of the Dasht-e-Bayaz (Iran) earthquake fractures. Geological Society of America Bulletin 81, 41–60.

Thoroddsen, Th., 1899. Jardskjalftar a Sudurlandi (Earthquakes in South Iceland), Hid íslenska Bókmenntafelag, Copenhagen.

Thoroddsen, Th., 1905. Large Earthquakes in Iceland, The Icelandic Literature Society, Copenhagen (in Icelandic).

Thoroddsen, Th., 1925. Die Geschichte der islandischen Vulkane, Memoir Royal Academy of Sciences, Denmark, Copenhagen.

Tryggvason, E., Thoroddsen, S., Thorarinson, S., 1958. Report on earthquake risk in Iceland. Journal of Engineer's Society of Iceland 43, 1–9 (in Icelandic).

Tryggvason, K., Husebye, E., Stefansson, R., 1983. Seismic image of the hypothesized Icelandic hot spot. Tectonophysics 100, 97–118.

Ward, P.L., 1971. New interpretation of the geology of Iceland. Geological Society of America Bulletin 82, 2991–3012.

Wells, D.L., Coppersmith, K.J., 1994. New empirical relationships among magnitude, rupture length, rupture width, rupture area, and surface displacement. Bulletin of the Seismological Society of America 84, 974–1002.